Korean J. Chem. Eng., 33(6), 1908-1916 (2016)
DOI: 10.1007/s11814-016-0018-5

pISSN: 0256-1115
eISSN: 1975-7220

Deep desulfurization of fuel gas by adsorption on Cu-impregnated activated carbons in practical conditions

Hoang Phuoc Ho*, Palraj Kasinathan*, Jaesung Kim, Doohwan Lee**,†, and Hee Chul Woo*,†**

*Department of Chemical Engineering, Pukyong National University, San 100 Yongdang-dong, Nam-gu, Busan 48547, Korea
**Department of Chemical Engineering, University of Seoul, 13 Siripdae-gil, Dongdaemun-gu, Seoul 02504, Korea
(*Received 13 November 2015 • accepted 17 January 2016*)

Abstract−Deep desulfurization properties and characteristics of activated carbon (AC) modified by impregnation of $CuCl_2$ were studied using simulated hydrocarbon fuels containing dimethyl sulfide (DMS), *tert*-butylmercaptan (TBM), and tetrahydrothiophene (THT), the typical organosulfur compounds representing sulfides, thiols, and thiophenes that exist in fuel gases. The pristine AC had limited adsorptive desulfurization performance for a ternary DMS-THT-TBM mixture feed with an early breakthrough of DMS and TBM due to its preferential adsorption of THT. The adsorption of these organosulfur species on the AC surface was intrinsically weak and competing, as indicated by their low desorption activation energies (37-39 kJ mol^{-1}). However, relatively stronger adsorption of THT than the others led to the AC surface gradually being covered by THT through replacement of the initially adsorbed TBM and DMS. The impregnation of $CuCl_2$ on the AC (3.4 atomic % Cu) additionally formed strong and selective adsorption sites for TBM (activation energy=58.6 kJ mol^{-1}) on the AC surface, which gave rise to about three-fold increase in the total breakthrough adsorption capacity for these sulfur species. The structure and physicochemical properties of the adsorbents were characterized by N_2 adsorption, x-ray diffraction, x-ray photoelectron spectroscopy, scanning electron microscopy, transmission electron microscopy, thermogravimetric analysis, differential scanning calorimetry, and surface pH measurement. The results suggested that the modulation of adsorption selectivity of the AC surface by $CuCl_2$ impregnation had significant effects on the overall deep desulfurization performance for fuel gases containing multiple organosulfur species in practical conditions.

Keywords: Adsorptive Desulfurization, Activated Carbon, Copper, Fuel Cell, Fuel Processing

INTRODUCTION

Deep desulfurization of hydrocarbon fuels is critically important in the catalytic production and purification of hydrogen for fuel cells, the prospective electrochemical system with versatile applicability in transportation and combined-heat-and-electric-power (CHP) generation [1]. Natural gas and biogas are practical and cost-effective feedstocks for hydrogen production that have multiple advantages, including extensive availability through a distribution network in urban areas, natural abundance, and renewability in the case of biogas [2]. These hydrocarbon fuels generally contain multiple organosulfur species, either naturally present or deliberately added at several ppm level for detection of a gas leak, which must be removed completely to prevent an irreversible and catastrophic deactivation of the Pt electrodes in fuel cell system [3]. Among various desulfurization methods, adsorptive desulfurization is simple and of high efficiency compared to conventional desulfurization processes such as hydrodesulfurization. Adsorptive desulfurization can provide deep desulfurization at ambient temperature and atmospheric pressure, which provides extensive advantages in the size, mobility, and practical operability for the fuel cell systems.

Several types of adsorbents, including zeolites [4-11], activated carbons [12-17], metal oxides [18-21], and the combination of these adsorbents [22] have been studied for adsorptive desulfurization of fuel gases. In particular, activated carbons (ACs) are versatile adsorbents with excellent physicochemical properties, including high surface area, microporous structure, and high degree of surface reactivity [23]. The low cost and greater regenerability also make activated carbons attractive, although zeolites may provide superior sulfur adsorption capacities [4-17]. Various studies have reported effective improvement of sulfur adsorption capacity of ACs, including the introduction of heteroatoms on the ACs [12,13,16,17] and the surface treatments to create acidic and basic groups [14,15]. Cui et al. studied adsorptive removal of dimethylsulfide (DMS) using activated carbon loaded with $FeCl_3$, which showed enhancement in DMS adsorption attributed to the interactions between the sulfur atom in DMS and the Fe species dispersed on the AC surface [12]. Kim et al. reported about two-fold increase in methyl mercaptan adsorption on AC after impregnation of $CuCl_2$, but details on the properties for their adsorptive interactions were not discussed [17]. Significantly, the previous studies dealt with the removal of a specific sulfur component, despite the presence of multiple organosulfur components in the fuels in practical condition. Therefore, thorough studies on the desulfurization performance of adsorbents, including adsorption capacity and selectivity in the presence of multiple organosulfur species, are necessary and

†To whom correspondence should be addressed.
E-mail: woohc@pknu.ac.kr, dolee@uos.ac.kr
‡This article is dedicated to Prof. Seong Ihl Woo on the occasion of his retirement from KAIST.

important to account for real desulfurization conditions.

We report here deep desulfurization performance and characteristics of $CuCl_2$ impregnated AC adsorbents (AC-$CuCl_2$) for a ternary mixture of organosulfur compounds, a mixture composed of dimethyl sulfide (DMS, C_2H_6S), *tert*-butylmercaptan (TBM, $C_4H_{10}S$), and tetrahydrothiophene (THT, C_4H_8S) balanced in methane. These components are the most common organosulfur species found in fuel gases and represent typical sulfide, thiol, and thiophene group compounds. The physicochemical properties of the AC-$CuCl_2$ adsorbents were characterized in detail, and their deep desulfurization properties were investigated with comparisons at different feed conditions, a single versus a ternary mixture of sulfur species. The adsorption capacity and selectivity of the AC-$CuCl_2$ for DMS, TBM, and THT were rationalized, identifying the adsorption sites for each sulfur species and their intrinsic adsorption strengths. These results demonstrated the specific roles of the Cu species impregnated on activated carbon for the modulation of deep desulfurization capacity and selectivity, providing insights on the essential factors for effective improvement of fuel desulfurization properties of activated carbons in practical conditions.

EXPERIMENTAL

1. Chemicals

Activated carbon (AC) powder derived from coconut shell (Katayama Chem) and copper chloride dihydrate ($CuCl_2 \cdot 2H_2O$, Junsei Chem.) were used for the preparation of the AC-$CuCl_2$ adsorbents. For the single organosulfur component feed gas, three different feeds containing one of the following, DMS (99.7 ppm), TBM (100.3 ppm), or THT (100.4 ppm), balanced in CH_4 (certified, Rigas) were used. For the ternary component simulated gas, an equimolar mixture of DMS (33.6 ppm), TBM (33.4 ppm), and THT (33.9 ppm) balanced in CH_4 was used for the sulfur adsorption experiments.

2. Preparation of Cu-impregnated AC Adsorbents

Activated carbon powder was used as the pristine AC without further chemical treatment. Copper was impregnated on the pristine AC in a rotary evaporator equipped with a condenser. In a typical synthesis, a 200 ml aqueous solution of $CuCl_2$ was prepared at different Cu concentrations (0.125-0.75 M). Then, 10 g of the pristine AC was immersed in the solution and mixed for 2 h at 353 K under atmospheric pressure, followed by 2 h of additional mixing at 308 K under vacuum with refluxing. The water was evaporated at 333 K for 0.5 h under vacuum, and the sample was further dried at 383 K for 12 h in a convection oven. The resulting sample was designated AC-$CuCl_2$-X, where X is the moles of Cu (0.25-1.5 mol-Cu g^{-1}) applied for impregnation on the pristine AC.

3. Characterization of Adsorbents

The structure of the pristine and the Cu-impregnated AC adsorbents was characterized by powder x-ray diffraction (XRD, X'pert-MPD, Philips). The spectra were obtained using graphite-monochromatized Cu K_α (λ=0.154 nm) radiation operated at 40 kV and 30 mA with a 2θ range from 10 to 80° at a scan rate of 4° min^{-1}. Nitrogen adsorption-desorption isotherms on the adsorbents were obtained in a volumetric unit (ASAP 2020, Micromeritics) after treatment of the sample under vacuum at 623 K for 3 h. The surface area of the samples was calculated by Brunauer-Emmett-Teller (BET) method, and the meso- and micro-porosities of the samples were determined by Barrett-Joyner-Halenda (BJH) and Horvath-Kawazoe (HK) methods, respectively.

Surface morphology of the adsorbents was characterized by scanning electron microscopy (SEM, S-2400, Hitachi) and high resolution transmission electron microscopy (HR-TEM, JEM-2010). Thermogravimetric analysis (TGA, TGA-7, Perkin Elmer) and differential scanning calorimetry (DSC, Pyris-1, Perkin Elmer) were employed to investigate the thermal and structural characteristics of the adsorbents. All the samples were carefully ground into fine power, and the temperature was increased from 323 to 873 K at a ramping rate of 10 K min^{-1} under inert N_2 flow. X-ray photoelectron spectroscopy (XPS, MultiLab-2000, Thermo Scientific) was conducted to obtain the total amount of Cu and the relative concentration of Cu (I) on the AC-$CuCl_2$ adsorbents. The spectra were taken after pretreatment of the sample in He at 573 K for 2 h. The surface acid-base properties of the adsorbents were indirectly determined by measuring pH of the sample suspension. Briefly, 0.4 g adsorbent was dispersed in 20 mL of distilled water and equilibrated overnight. The sample was filtered and the pH of solution was measured with a pH meter [14].

4. Sulfur Adsorption Uptake Measurement

Sulfur adsorption uptake of the pristine and the AC-$CuCl_2$ adsorbents was measured at 298 K in a fixed-bed glass reactor (I.D= 4 mm) packed with 30 mg adsorbent at atmospheric pressure. The adsorption was measured *in-situ* with three sequential steps: pretreatment, adsorption, and desorption. In pretreatment, the sample was treated at 723 K for 2 h in flowing He (99.999%) and cooled to room temperature. In the adsorption step, a simulated gas containing the organosulfur species in CH_4 was fed to the reactor at a constant flow rate of 50 mL min^{-1} (STP). The concentration of the sulfur species in the effluent was measured online by using a gas chromatograph (GC, HP 5890 II) equipped with a capillary column (HP-1, 30 m - 0.32 mm - 0.25 μm) and a flame ionization detector (FID). The adsorption measurement was terminated when the effluent concentration of the sulfur species was equalized with the feed concentration. Breakthrough adsorption capacity was defined as the amount of sulfur species adsorbed before its detection in the effluent by FID (detection limit≈0.1 ppm). This was calculated for each organosulfur species according to the following equation:

$$S\ (\text{mmol g}^{-1}) = \frac{Q\ (\text{mL min}^{-1}) \times t\ (\text{min}) \times C_o\ (\text{ppm}) * 10^{-6}}{22.400\ (\text{mL mmol}^{-1}) \times m_{ads}\ (\text{g})} \quad (1)$$

where S is breakthrough adsorption capacity (mmol-S g^{-1}) for each organosulfur species, C_o is the inlet concentration (ppm-S) of sulfur species, Q is the volumetric flow rate (ml min^{-1}, STP) of feed, t is the breakthrough time (min), and m_{ads} is the mass (g) of the adsorbent.

After the adsorption measurement was finished, thermal desorption characteristics of the sulfur species were obtained by temperature programmed desorption (TPD) method. The spent adsorbent was purged in flowing He at 303 K for 1 h, and the sample temperature was raised to 773 K (ramping rate=10 K min^{-1}) in flowing He (50 ml min^{-1}, STP). The desorption of DMS, TBM, and THT was analyzed online by using a quadrupole mass spectrometer (HPR 20, Hiden Analytical).

5. Desorption Activation Energy

TPD can provide valuable information regarding the characteristics of adsorbate - adsorbent interactions and activation energy for desorption [24]. According to Cvetanovic et al. [25], the desorption activation energy can be determined by

$$\log\left(\frac{T_m^2}{\beta}\right)=\frac{E_d}{2.303RT_m}+\log\left(\frac{E_d}{RA}\right) \quad (2)$$

where T_m is the temperature of desorption maximum (K), β is the heating rate (K min^{-1}), E_d is the desorption activation energy (kJ mol^{-1}), R is the gas constant, and A is an index representing the argument. The temperature of desorption maximum (T_m) was obtained as a function of heating rate (β), and then a linear regression of the experimental data allowed quantitative estimation of the desorption activation energy of the species from its slope. This procedure was conducted for the pristine AC and the AC-$CuCl_2$ adsorbents using the single sulfur component feed gas (DMS, TBM or THT balanced in methane). The details of the experimental procedure can be found elsewhere [10].

RESULTS AND DISCUSSION

1. Characterization of Adsorbents

Fig. 1 shows the XRD patterns of the ACs with different loading amounts of $CuCl_2$. All the samples exhibited amorphous structures with two broad diffraction peaks at around 24° and 43°, which is typical for amorphous ACs. No diffraction peaks attributed to crystalline Cu species were observed, indicating that the impregnated $CuCl_2$ was highly dispersed. Fig. 2(a) displays the N_2 adsorption - desorption isotherms on the AC adsorbents of different Cu loadings. All the isotherms were similar and exhibited type I according to IUPAC classification, which is typical for microporous activated carbon materials. The pore size distributions on the samples calculated by Horvath-Kawazoe (Fig. 2(b)) and Barrett-Joyner-Halenda (Fig. 2(c)) methods indicated the co-presence of micro and mesopores on the samples to substantial amounts. It was noticeable that the proportion of micropores (Fig. 2(b)) on the samples gradually decreased with an increase in the $CuCl_2$

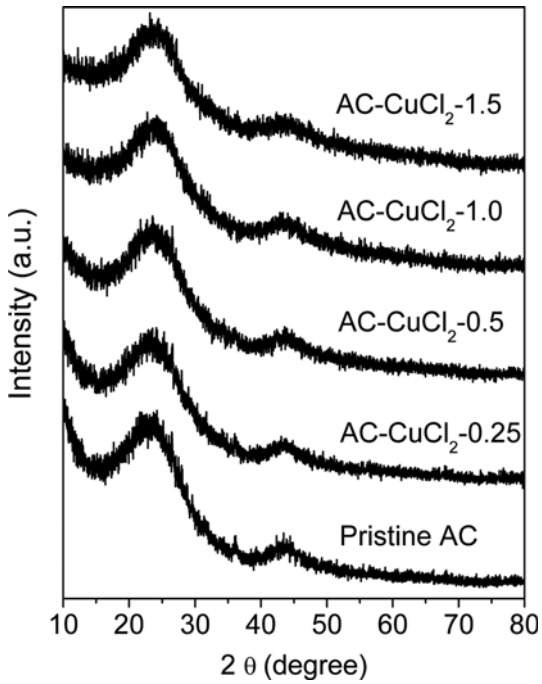

Fig. 1. XRD patterns of the pristine AC and the Cu-impregnated AC adsorbents.

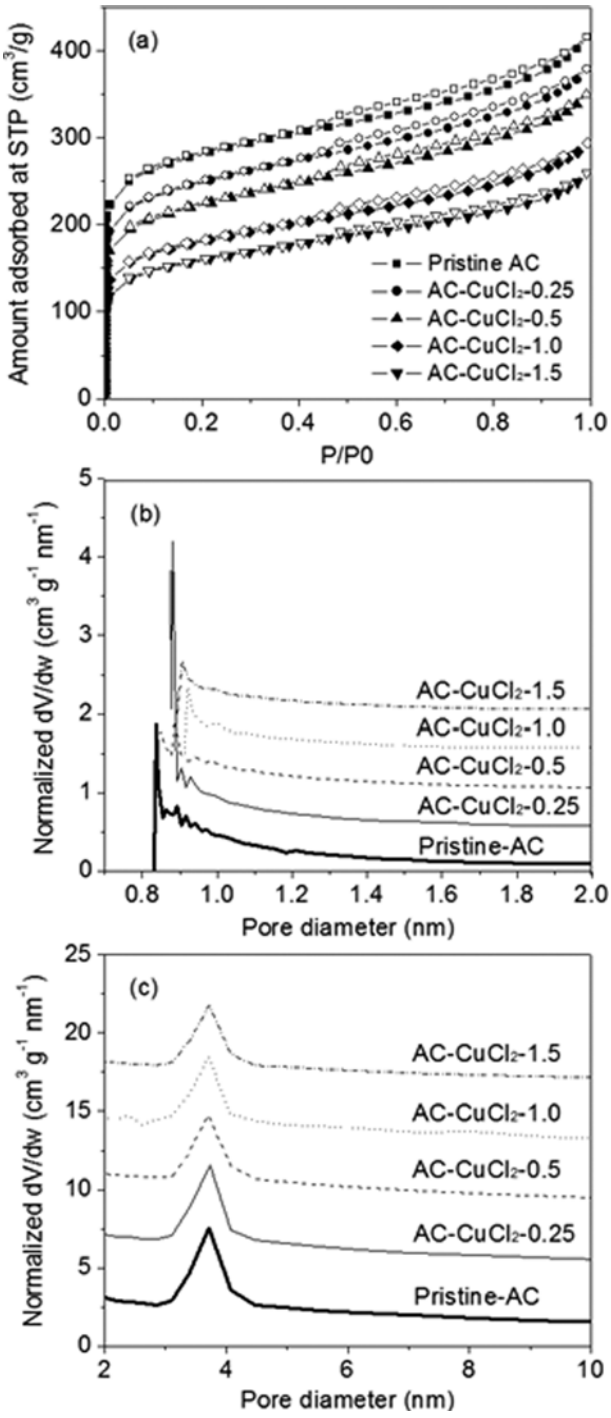

Fig. 2. N_2 adsorption - desorption isotherm (a), size distribution of micropores (b), and size distribution of mesopores (c) on the pristine AC and the Cu-impregnated AC adsorbents.

Table 1. Surface area, pore volume, and average pore size of the pristine AC and the AC-$CuCl_2$-1.0 adsorbents

Adsorbent	BET surface area ($m^2\ g^{-1}$)				Pore volume ($cm^3\ g^{-1}$)				Average micropore size (nm)
	S_{Total}	S_{Micro}	S_{Meso}	S_{Micro}/S_{Meso}	V_{Total}	V_{Micro}	V_{Meso}	V_{Micro}/V_{Meso}	
Pristine AC	917	708	209	3.4	0.65	0.36	0.29	1.2	1.02
AC-$CuCl_2$-0.25	784	571	213	2.7	0.59	0.36	0.23	1.5	1.04
AC-$CuCl_2$-0.5	686	474	212	2.2	0.54	0.26	0.28	1.0	1.06
AC-$CuCl_2$-1.0	541	357	184	1.9	0.46	0.21	0.25	0.9	1.10
AC-$CuCl_2$-1.5	470	315	155	2.0	0.40	0.19	0.22	0.9	1.12

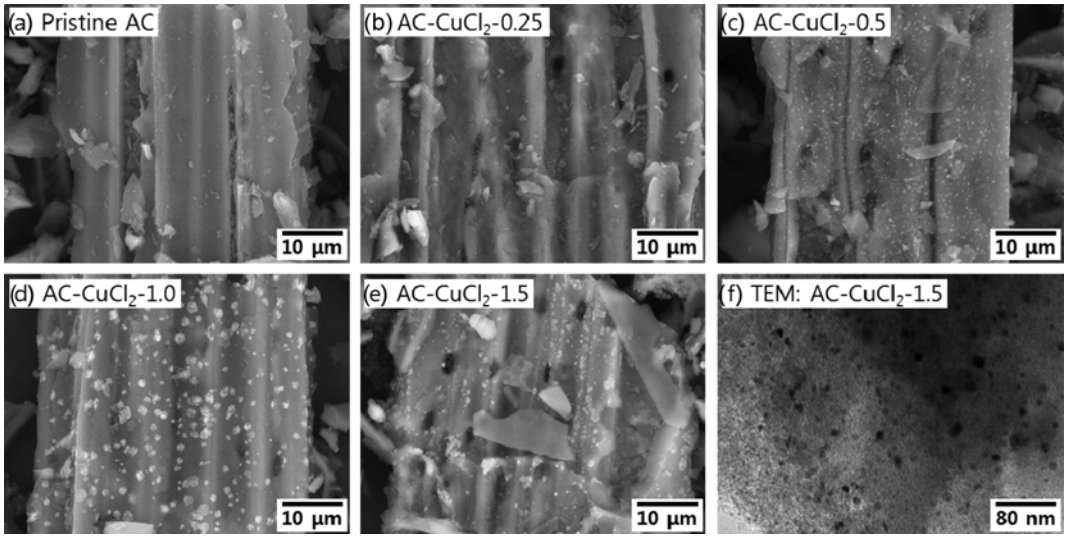

Fig. 3. SEM (a)-(e) and TEM (f) micrographs of the AC-$CuCl_2$ adsorbents with different Cu loading amounts.

impregnation amount due to occurrence of pore blockage. Differently, the amount and size distribution of the mesopores (Fig. 2(c)) were little affected by the impregnation. Table 1 shows the average pore size, surface area, and pore volume of the adsorbents in detail. The average size of the micropores and the mesopores on the AC-$CuCl_2$ adsorbents was 1.02-1.12 nm and 3.7 nm, respectively. A gradual decrease of the overall surface area and pore volume was observed with an increase in the $CuCl_2$ loading, preferentially on the micropores as indicated by the micorpore/mesopore surface area and volume ratios.

Fig. 3 shows the SEM (3(a)-3(e)) and TEM (3(f)) micrographs of the pristine AC and the AC-$CuCl_2$ adsorbents. The pristine AC exhibited a relatively clean surface with some AC debris broken from the bulk structure, and the same was observed on the AC-$CuCl_2$-0.25 with low $CuCl_2$ loading. The Cu species could not be observed clearly on AC-$CuCl_2$-0.25, suggesting a fine dispersion of Cu on the surface (3(b)). A number of small $CuCl_2$ particles in sizes of several tens nm dispersed on the AC surface began to appear

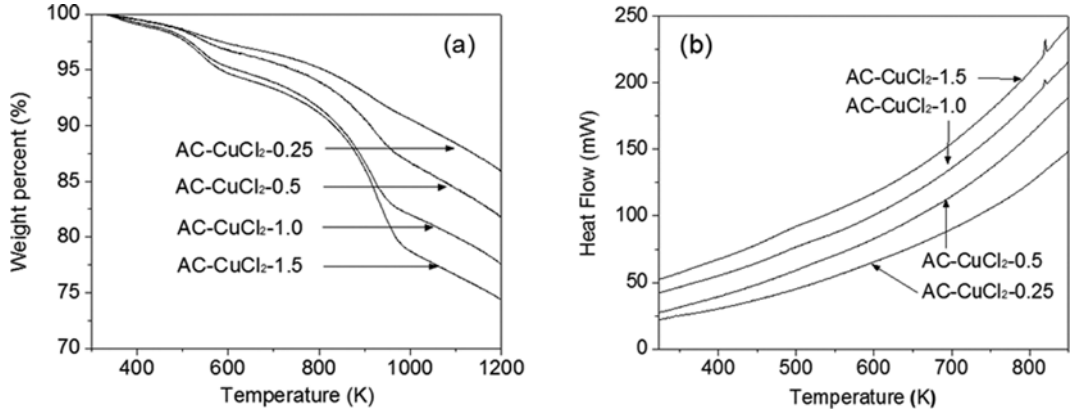

Fig. 4. TGA (a) and DSC (b) analysis results on the AC-$CuCl_2$ adsorbents with different Cu loading amounts.

on the AC-$CuCl_2$-0.5 (3(c)). The high dispersion of $CuCl_2$ particles was also observed on AC-$CuCl_2$-1.0 and AC-$CuCl_2$-1.5 samples, but these particles resided on the surface as clusters (3(d)-3(e)). The TEM micrograph (3(f)) of the AC-$CuCl_2$-1.5 presented a clear aspect on the high dispersity of these particles, in which a number of nanoparticles with sizes of several tens nm were finely dispersed on this highly Cu loaded sample.

Thermal and structural characteristic of the AC-$CuCl_2$ adsorbents were investigated by TGA and DSC analysis. Fig. 4 displays the TGA (4(a)) and DSC (4(b)) results on the AC-$CuCl_2$ adsorbents with different Cu loadings. A slight weight loss (3-5 wt%) was observed below 473 K on all the samples, which was attributed to desorption of adsorbed water species. The AC-$CuCl_2$ samples exhibited an extensive and stepwise weight loss between 473 and 1,073 K due to progressive thermal reduction of the Cu species ($CuCl_2 \rightarrow CuCl \rightarrow Cu$) [26], which was proportional to the $CuCl_2$ impregnation amounts. The DSC results (Fig. 4(b)) indicated that recrystallization of Cu species occurred on AC-$CuCl_2$-1.0 and AC-$CuCl_2$-1.5 after the thermal reduction, as evidenced by the peak at ~813 K. This was not observed on the samples with low $CuCl_2$ loadings (AC-$CuCl_2$-0.25 and AC-$CuCl_2$-0.5), which was likely due to the high dispersity of Cu species on the AC surface.

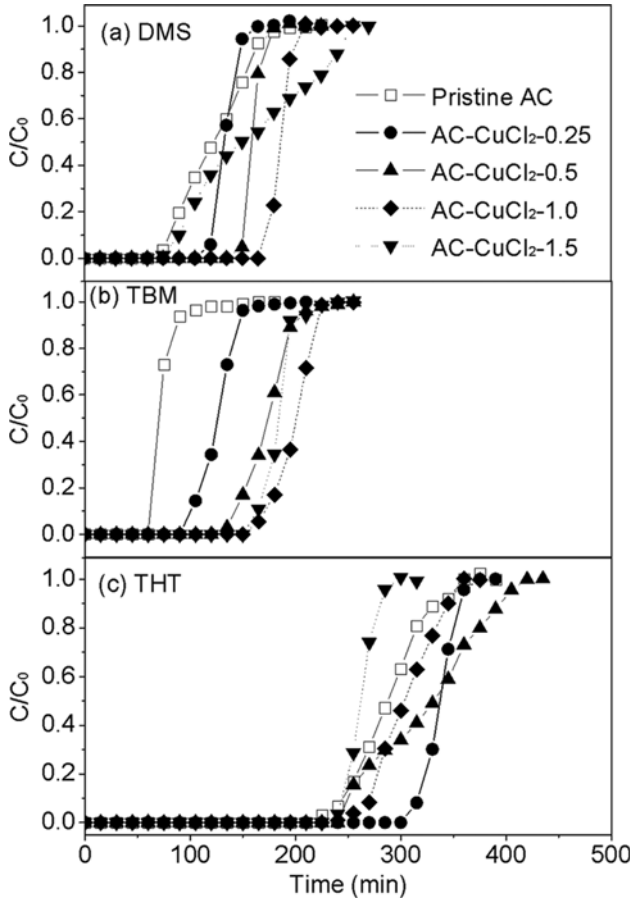

Fig. 5. Time-on-stream desulfurization performance of the pristine AC and the AC-$CuCl_2$ adsorbents for single sulfur component of DMS (a), TBM (b), and THT (c) on the stream (100 ppm-S in CH_4 balance) at 298 K.

2. Effects of $CuCl_2$ Loading on Desulfurization Properties

Fig. 5 shows the time-on-stream desulfurization performance of the pristine AC and the AC-$CuCl_2$ adsorbents for DMS, TBM, and THT, which was fed as a single organosulfur component balanced in CH_4 stream (100 ppm-S). The breakthrough adsorption capacity of the adsorbents was calculated (Eq. (1)) and the results are summarized in Table 2. All these adsorbents exhibited higher breakthrough adsorption capacity for THT than for DMS and TBM. Note that the AC-$CuCl_2$ adsorbents exhibited substantially greater desulfurization performance than the pristine AC for TBM and DMS, suggesting constructive contributions of the impregnated

Table 2. Breakthrough adsorption capacity of the pristine AC and the AC-$CuCl_2$ adsorbents for three different single component feeds of DMS, TBM, and THT at 298 K (each feed contains 100 ppm-S in CH_4 balance)

Sample	Breakthrough adsorption capacity (mmol-S g^{-1})		
	DMS	TBM	THT
Pristine AC	0.47	0.46	1.56
AC-$CuCl_2$-0.25	0.81	0.68	2.29
AC-$CuCl_2$-0.5	1.02	0.88	1.83
AC-$CuCl_2$-1.0	1.16	1.16	1.74
AC-$CuCl_2$-1.5	0.58	1.13	1.64

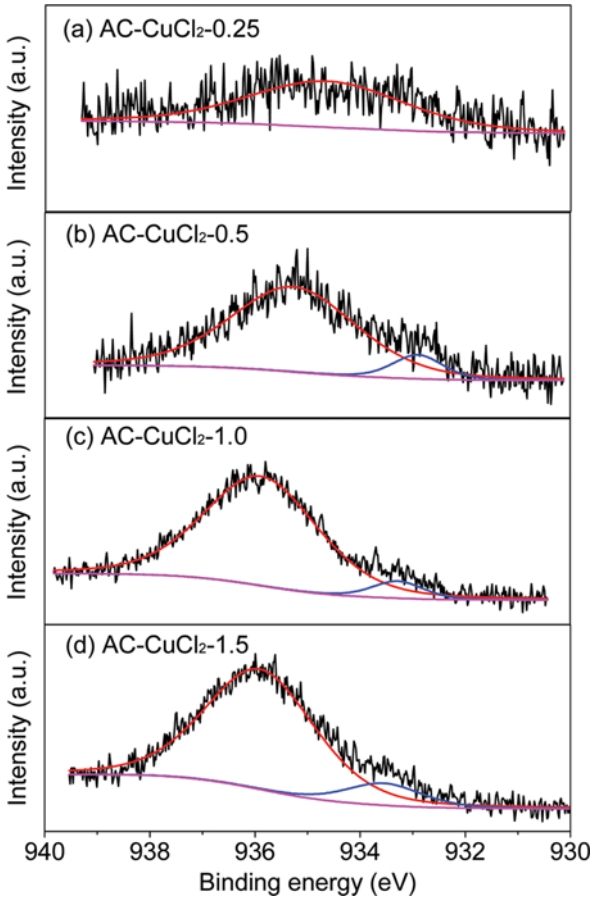

Fig. 6. XPS Cu2$p_{3/2}$ spectra of the AC-$CuCl_2$ adsorbents with different Cu impregnation amounts.

Table 3. Atomic composition, surface pH, and relative amount of Cu(I) in the total Cu species dispersed on the AC-$CuCl_2$ adsorbents

Sample	Atomic composition (%)				Surface pH	Cu(I)/[Cu(I)+Cu(II)] atomic ratio (%)
	Cu	Cl	O	C		
Pristine AC	0	0	6.9	93.1	4.8	-
AC-$CuCl_2$-0.25	0.6	1.2	7.9	90.3	4.1	0
AC-$CuCl_2$-0.5	1.1	2.4	8.8	87.7	4.0	10.3
AC-$CuCl_2$-1.0	3.4	4.4	11.7	80.5	3.9	8.7
AC-$CuCl_2$-1.5	3.2	4.0	9.5	83.3	3.9	11.3

$CuCl_2$ species for selective sulfur adsorption. The breakthrough adsorption capacity for DMS increased with $CuCl_2$ impregnation, showing a maximum on AC-$CuCl_2$-1.0 with a capacity value approximately 2.5-times larger than that on the pristine AC. However, excessive $CuCl_2$ loading had detrimental effects, as shown by the early occurrence of DMS breakthrough on AC-$CuCl_2$-1.5 (Fig. 5(a)). The breakthrough adsorption capacity for TBM showed a gradual increase with $CuCl_2$ loading amount and reached a highest value on AC-$CuCl_2$-1.0 and AC-$CuCl_2$-1.5 samples. However, $CuCl_2$ impregnation had little effect on the breakthrough adsorption capacity for THT; a moderate increase of THT adsorption occurred only on the AC-$CuCl_2$-0.25 with low $CuCl_2$ loading.

The considerable enhancements in the deep desulfurization performance of the AC-$CuCl_2$ adsorbents suggested the constructive roles of the impregnated Cu species for the selective organosulfur adsorption. The enhancements were due to the direct interactions between the sulfur atom of the compounds and the Cu species on the AC surface, rather than π-complexation which is known to occur between Cu (I) and cyclic organosulfur species having double bonds such as thiophene [27]. Fig. 6 displays the $Cu2p_{3/2}$ XPS spectra on the AC-$CuCl_2$ samples of different $CuCl_2$ loading amount. The samples exhibit a major absorption band at biding energy of 935.4 eV, which is attributed to Cu(II) species. An additional small absorption band appears at 933.2 eV and the intensity increases with an increase in $CuCl_2$ loading, which is attributed to the partially reduced Cu(I) species on the samples [28]. Table 3 shows the atomic composition of the major heteroatoms and the relative amount of Cu(I) in the overall Cu species dispersed on the sample surface. The presence of Cu, Cl, and O species was mainly observed on the AC-$CuCl_2$ samples. The results confirmed a gradual increase in the overall Cu loading amount, reaching a maximum of 3.4 atomic percent Cu on the AC-$CuCl_2$-1.0. The surface concentration of Cl and O atoms concomitantly increased, also reaching a maximum on the AC-$CuCl_2$-1.0. The acidity was highest on this sample, likely due to acidic oxygen species introduced on the surface. On the other hand, the relative concentration of Cu(I) was similar on these AC-$CuCl_2$ samples, with an approximate value of 10%. The exception was for the AC-$CuCl_2$-0.25, which displayed a minor presence of Cu(I) species. The Cu(I) species were likely formed via autothermal reduction by the thermal pretreatment at 573 K. Note that the enhancements in breakthrough adsorption capacity of the AC-$CuCl_2$ adsorbents for DMS, TBM, and THT were not primarily caused by the Cu(I) species, different from the superior desulfurization performance of Cu(I) species reported for thiophenes. The results are reasonable, considering that DMS, TBM, and THT are saturated molecules that are incapable of the π-complexation with Cu(I) species. Therefore, the high desulfurization performance of AC-$CuCl_2$ for TBM and DMS was attributed to the direct interactions between the sulfur atoms in these molecules and the Cu species on the AC surface. This was also reasonable, considering that the breakthrough order of these sulfur compounds (DMS>TBM>THT) followed the order of steric hindrance expected for these molecules (DMS>TBM>THT).

3. Effect of Cu on the Desorption Characteristic of Sulfur Compounds

The adsorptive interaction of DMS, TBM, and THT on the

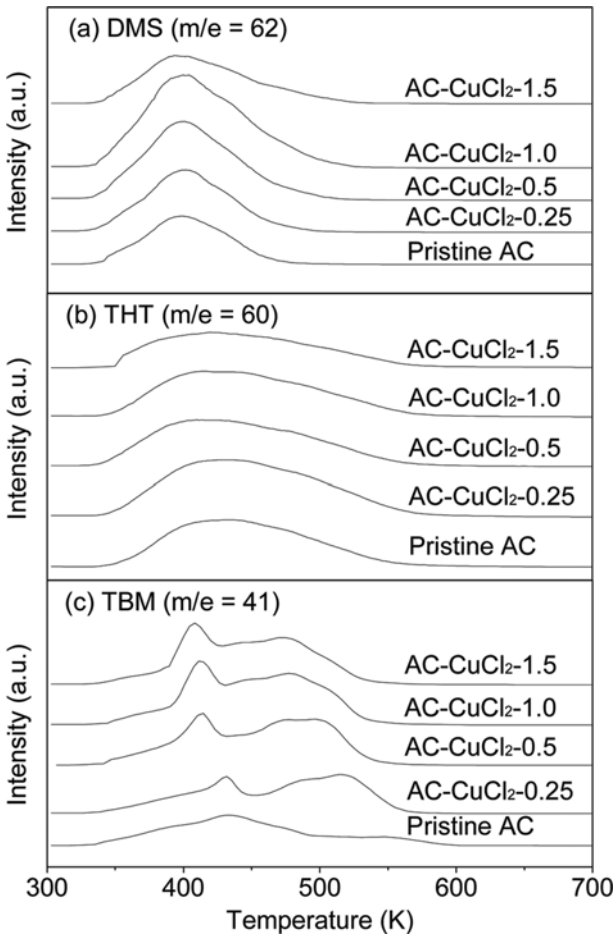

Fig. 7. Temperature programmed desorption (TPD) profiles of DMS (a), THT (b), and TBM (c) on the pristine AC and the AC-$CuCl_2$ adsorbents.

pristine AC and the AC-$CuCl_2$ adsorbents was characterized by temperature programmed desorption (TPD) of these species. Fig. 7 displays the TPD results. On the TPD of DMS (Fig. 7(a)), the dominant desorption fragments were $(CH_3)_2S$ (m/e=62) and CH_3S (m/e=47). The pristine AC displayed a nearly symmetric desorption band of DMS (m/e=62) with a peak maximum approximately at 400 K. The same feature was observed on the CH_3S (m/e=47) fragment. The AC-$CuCl_2$ adsorbents also exhibited desorption maxima approximately at 400 K, similar to the pristine AC. However, an additional DMS desorption peak appeared slightly at ~479 K and its intensity increased a little with an increase in the $CuCl_2$ loading, indicating formation of some additional adsorption sites for DMS with the $CuCl_2$ impregnation. On the TPD of THT (Fig. 7(b)), the major desorption species were $(CH_2)_4S$ (m/e=88) and C_2H_4S (m/e=60). These fragments had the same TPD feature, displaying a broad peak ranging from 353 to 563 K with the peak maximum at ~433 K. A similar TPD pattern on the pristine AC and the AC-$CuCl_2$ adsorbents, not depending on the Cu loading amount, clearly indicated that the impregnation of $CuCl_2$ had little effect on THT adsorption. The TPD of TBM (Fig. 7(c)) gave rise to a completely different feature on the AC-$CuCl_2$ samples. On the pristine AC, the TBM desorption (m/e=41) mainly occurred with a single desorption peak at ~435 K. On the AC-$CuCl_2$ samples, new desorption peaks appeared strongly at elevated temperatures of 473-513 K, indicating the presence of additional adsorption sites for TBM with strong adsorption strength. These results collectively suggest that an introduction of Cu by impregnation of $CuCl_2$ on the pristine AC had substantial effects on the TBM adsorption properties, while it had little effect on the THT adsorption.

4. Adsorption Strength of the Species on the Adsorbents

The relative adsorption strength of DMS, THT, and TBM on the pristine AC and the AC-$CuCl_2$ adsorbents was estimated from the desorption activation energies of these species that were obtained by applying the Eq. (2) on the TPD results. Fig. 8 shows the linear regression ($\log(T_m^2/\beta)$ vs. $1/T_m$) results and the desorption activation energy of DMS, TBM, and THT on the pristine AC (Fig. 8(a)) and the AC-$CuCl_2$-1.0 (Fig. 8(b)). The results display excellent linear correlation 5 for these organosulfur species. The pristine AC had similar and relatively low activation energies for these species (DMS=37.8, TBM=37.0, THT=38.9 kJ mol^{-1}). The activation energy for DMS and THT desorption on the AC-$CuCl_2$-1.0 (DMS=39.0, THT=39.5 kJ mol^{-1}) varied little from that on the pristine AC, agreeing with the TPD results which suggested that the introduced Cu species had little effect on the adsorption of these species. Two different values of TBM desorption activation energies (42.1 and 58.6 kJ mol^{-1}) were obtained, corresponding to the

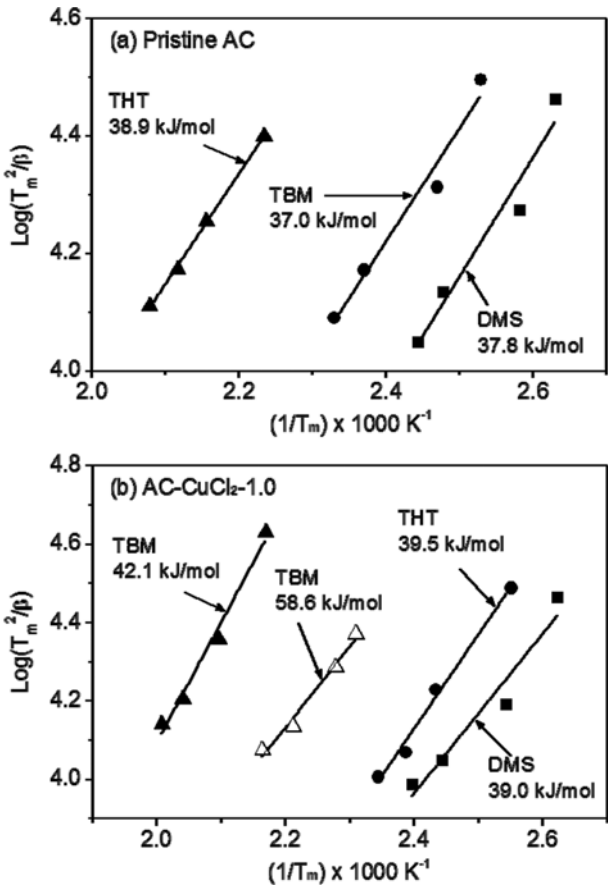

Fig. 8. Liner regression analysis results of $\log(T_m^2/\beta)$ vs. $(1/T_m)$ and the desorption activation energy of DMS, TBM, and THT on the pristine AC (a) and the AC-$CuCl_2$-1.0 (b).

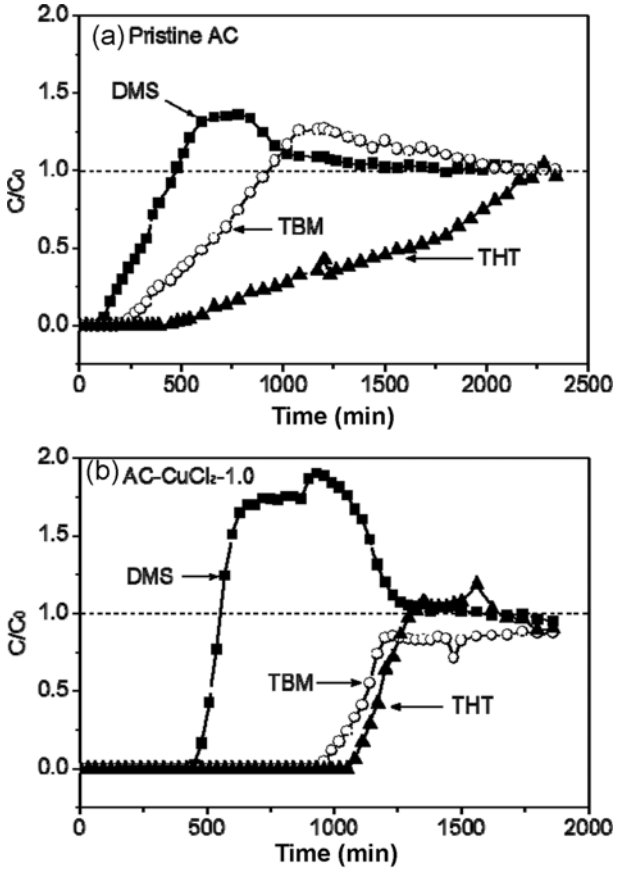

Fig. 9. Time-on-stream desulfurization performance of the pristine AC (a) and the AC-$CuCl_2$-1.0 (b) for an equimolar ternary mixture of DMS, TBM, and THT (total 101 ppm-S in CH_4 balance) at 298 K.

two distinct desorption peaks at 423 and 500 K on the AC-$CuCl_2$-1.0: the first attributed to the AC surface and the second to the impregnated Cu species. The results clearly show that the impregnated Cu species provided new adsorption sites of high adsorption strength for TBM. This markedly affected not only the adsorption selectivity of TBM but also the overall desulfurization characteristics for a ternary component (DMS-TBM-THT) mixture.

5. Adsorption Selectivity

Adsorption selectivity of the pristine AC and the AC-$CuCl_2$-1.0 for DMS, TBM, and THT was investigated using an equimolar ternary mixture feed (DMS=33.6, TBM=33.4, THT=33.9 ppm, CH_4 balanced). Fig. 9 shows the time-on-stream desulfurization performance of the adsorbents. The desulfurization characteristics of the adsorbents for the ternary mixture were largely different from that for the single sulfur species. The pristine AC (Fig. 9(a)) had initial uptake for all these organosulfur species, but the weakly adsorbed DMS and TBM species began to desorb with time on the stream accompanying a continuous adsorption of THT. The results reflected that THT molecules progressively displaced the adsorbed DMS and TBM on the pristine AC surface. The results suggest that (i) DMS, TBM, and THT compete for the same adsorption sites on the pristine AC surface, and that (ii) THT has higher adsorption affinity than TBM and DMS on these adsorption sites. The results agree well with the higher desorption temperature of THT observed in the TPD analysis (Fig. 7) and the higher desorption activation energy of THT compared to TBM and DMS (Fig. 8).

The impregnation of $CuCl_2$ on the AC surface resulted in significant changes in the adsorption characteristics of DMS, TBM, and THT in the ternary mixture feed stream (Fig. 9(b)). The AC-$CuCl_2$-1.0 adsorbent had initial adsorption uptake for all these species. However, the induced desorption occurred only for DMS with time on the stream accompanying continuous THT and TBM uptakes. The results accounted for the selective TBM adsorption on the sites additionally formed on the AC surface by the $CuCl_2$ impregnation. The much greater desorption activation energy of TBM on these adsorption sites (58.6 kJ mol^{-1}) clarifies that TBM strongly and preferentially adsorbed on the dispersed Cu species (Fig. 8(b)) on the AC-$CuCl_2$ adsorbent. However, note that desorption activation energy of DMS and THT on the AC-$CuCl_2$-1.0 (DMS=39.0, THT=39.5 kJ mol^{-1}) was practically the same as that on the pristine AC (DMS=37.8, THT=38.9 kJ mol^{-1}), indicating that the interactions of THT and DMS with the Cu on the adsorbent were relatively negligible.

Table 4 summarizes the overall breakthrough adsorption capacities of the pristine AC and the AC-$CuCl_2$-1.0 for the equimolar ternary mixture of DMS, TBM, and THT. The results showed 3.3-times greater total breakthrough adsorption capacity of the AC-$CuCl_2$ than the pristine AC due to the impregnation of the Cu species on the AC surface. The increment was highest for TBM (4.6-times) followed by DMS (4.0-times) and THT (2.6-times). The results are reasonable in that the impregnated Cu species offered preferential TBM adsorption. This would in turn allow a substantial increment of DMS breakthrough adsorption by providing more vacant sites on the AC surface to accommodate the competing DMS molecules. The increase of THT breakthrough adsorption on the AC-$CuCl_2$ was likely due to the increased acidity on the AC surface, which has been reported to preferentially promote THT adsorption over TBM [14]. The results are promising in that the selective TBM adsorption on the Cu species not only increased the TBM breakthrough adsorption but also gave rise to about three-fold increase in the total desulfurization performance of the pristine AC in the ternary organosulfur mixture feed.

Regenerability of the adsorbents was investigated by thermally regenerating the spent samples in flowing He at 723 K for 3 h. The results for the pristine AC and the AC-$CuCl_2$-1.0 adsorbent are compared in Table 4. The results show that the pristine AC had an excellent thermal regenerability with only about 9% loss in the total breakthrough adsorption capacity after the thermal regeneration. In contrast, the AC-$CuCl_2$-1.0 suffered from a relatively greater deactivation by the thermal regeneration with about 45% decrease in the total breakthrough adsorption capacity from 2.24 to 1.23 mmol-S g^{-1}. The deactivation could be explained by aggregation and phase transition of the impregnated Cu species by thermal regeneration. Fig. 10 shows the XRD pattern of the fresh and the regenerated AC-$CuCl_2$-1.0 samples. The results clearly indicate that the Cu species was finely dispersed on the fresh sample.

Table 4. Breakthrough adsorption capacity of the fresh and the thermally regenerated adsorbents for a ternary mixture of DMS, TBM, and THT at 298 K (Feed=33.6 ppm DMS, 33.4 ppm TBM, and 33.9 ppm THT, in CH_4 balance). The regeneration was conducted by flowing He at 723 K for 3 h

Adsorbent		Breakthrough adsorption capacity (mmol-S g^{-1})			
		DMS	TBM	THT	Total
Fresh	Pristine AC	0.10	0.19	0.38	0.67
	AC-$CuCl_2$-1.0	0.40	0.87	0.97	2.24
Regenerated	Pristine AC	0.09	0.17	0.35	0.61
	AC-$CuCl_2$-1.0	0.20	0.48	0.56	1.23

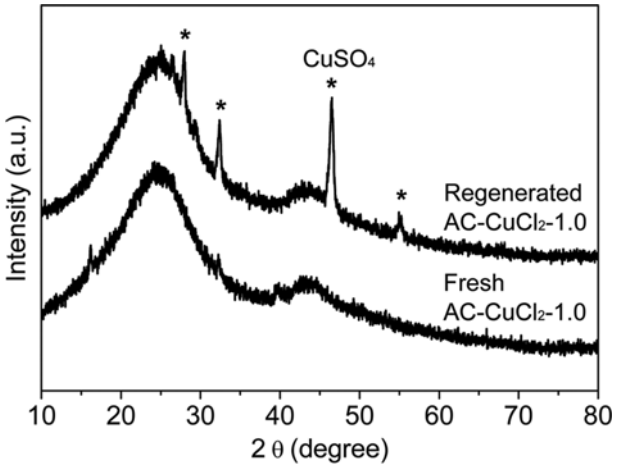

Fig. 10. XRD pattern of the fresh and the regenerated AC-$CuCl_2$-1.00 adsorbent (the regeneration was carried out in flowing He at 723 K for 3 h). The peaks (*) on the regenerated sample corresponds to the crystalline $CuSO_4$ particles (JCPDS #77-1900).

The formation of crystalline $CuSO_4$ particles was identified on the regenerated AC-$CuCl_2$-1.0, which occurred via reactions of the dispersed Cu species with the adsorbed organosulfur species by the thermal regeneration treatment.

CONCLUSIONS

Deep desulfurization performance of activated carbon for gases fuels depends on its adsorption capacity and selectivity toward various organosulfur components in the feed stream. The pristine AC has preferential adsorption for THT in a ternary DMS-THT-TBM mixture (representing typical sulfides, thiophenes, and thiols), which limits the overall desulfurization performance, displaying an induced desorption of the initially adsorbed TBM and DMS species from the AC surface via a concomitant displacement by the strongly adsorbing THT molecules. Impregnations of Cu species on the AC surface gave rise to formation of the preferential TBM adsorption sites, which allowed significant increase in the breakthrough adsorption capacity both for TBM and DMS by decoupling the competitive adsorption of these species on the AC surface. The AC-$CuCl_2$-1.0 (3.4 atomic % Cu on the surface) had about three-fold greater total breakthrough adsorption capacity than the pristine AC, which suggests that the modulation of adsorption selectivity by Cu impregnation can have marked constructive effects on the overall deep desulfurization of fuel gases by activated carbons in practically relevant conditions.

ACKNOWLEDGEMENTS

H. C. Woo acknowledges the support by Basic Science Research Program through the National Research Foundation of Korea funded by the Ministry of Education (NRF-2013R1A1A4A01007792). D. Lee acknowledges the financial support from University of Seoul (2015 Research Fund).

REFERENCES

1. J. Andrews and B. Shabani, *Int. J. Hydrogen Energy*, **37**, 1184 (2012).
2. W. Vielstich, A. Lamm and H. A. Gasteiger, *Handbook of Fuel Cells - Fundamentals, Technology and Applications*, Wiley, New York (2003).
3. X. Ma, L. Sun and C. Song, *Catal. Today*, **77**, 107 (2002).
4. H. Wakita, Y. Tachibana and M. Hosaka, *Micropor. Mesopor. Mater.*, **46**, 237 (2001).
5. S. Satokawa, Y. Kobayashi and H. Fujiki, *Appl. Catal. B: Environ.*, **56**, 51 (2005).
6. C.-L. Hwang and N.-H. Tai, *Appl. Catal. B: Environ.*, **93**, 363 (2010).
7. D. Lee, J. Kim, H. C. Lee, K. H. Lee, E. D. Park and H. C. Woo, *J. Phys. Chem. C*, **112**, 18955 (2008).
8. D. Lee, E.-Y. Ko, H. C. Lee, S. Kim and E. D. Park, *Appl. Catal. A: Gen.*, **334**, 129 (2008).
9. P. H. Ho, S. C. Lee, J. Kim, D. Lee and H. C. Woo, *Fuel Process. Technol.*, **131**, 238 (2015).
10. G. S. Jung, D. H. Park, D. H. Lee, H. C. Lee, S. B. Hong and H. C. Woo, *Appl. Catal. B: Environ.*, **100**, 264 (2010).
11. Y. H. Kim, H. C. Woo, D. Lee, H. C. Lee and E. D. Park, *J. Korean Eng.*, **26**, 1291 (2009).
12. H. Cui and S. Q. Turn, *Appl. Catal. B: Environ.*, **88**, 25 (2009).
13. H. Cui, S. Q. Turn and M. A. Reese, *Energy Fuels*, **22**, 2550 (2008).
14. P. H. Ho, S.-Y. Lee, D. Lee and H.-C. Woo, *Int. J. Hydrogen Energy*, **39**, 6737 (2014).
15. H. Tamai, H. Nagoya and T. Shiono, *J. Colloid Interface Sci.*, **300**, 814 (2006).
16. S. Bashkova, A. Bagreev and T. J. Bandosz, *Langmuir*, **19**, 6115 (2003).
17. D. J. Kim and J. E. Yie, *J. Colloid Interface Sci.*, **283**, 311 (2005).
18. H.-T. Kim, S.-M. Kim, K.-W. Jun, Y.-S. Yoon and J.-H. Kim, *Int. J. Hydrogen Energy*, **32**, 3603 (2007).
19. S.-H. Kang, J.-W. Bae, H.-T. Kim, K.-W. Jun, S.-Y. Jeong and K. V. R. Chary, *Energy Fuels*, **21**, 3537 (2007).
20. C. H. Ko, H.-I. Song, J.-H. Park, S.-S. Han and J.-N. Kim, *Korean J. Chem. Eng.*, **24**, 1124 (2007).
21. P. H. Ho, S. C. Lee, J. Kim, D. Lee and H. C. Woo, *Korean J. Chem. Eng.*, **32**, 1766 (2015).
22. C. Ratnasamy, J. P. Wagner, S. Spivey and E. Weston, *Catal. Today*, **198**, 233 (2012).
23. R. C. Bansal and M. Goyal, *Activated carbon adsorption*, CRC Press, Florida (2005).
24. I. M. Richard, *Principles of adsorption and reaction on solid surfaces*, Wiley-Interscience, New York (1996).
25. R. J. Cvetanović and Y. Amenomiya, *Adv. Catal.*, **17**, 103 (1967).
26 G. Mul, F. Kapteijn and J. A. Moulijn, *Appl. Catal. B: Environ.*, **12**, 33 (1997).
27. R. T. Yang, A. J. Hernandez-Maldonado and F. H. Yang, *Science*, **301**, 79 (2003).
28. J. F. Moulder, W. F. Stickle, P. E. Sobol, K. D. Bomben, J. Chastain and R. C. King, *Hanbook of X-ray Photoelectron Spectroscopy*, Physical Electronic Division, U.S.A. (1995).